Eur. Phys. J. B **39**, 483–489 (2004)
DOI: 10.1140/epjb/e2004-00221-y

THE EUROPEAN PHYSICAL JOURNAL B

Ultrafast creation and annihilation of space-charge domains in a semiconductor superlattice observed by use of Terahertz fields

F. Klappenberger[1,a], K.N. Alekseev[1,b], K.F. Renk[1], R. Scheuerer[1], E. Schomburg[1], S.J. Allen[2], G.R. Ramian[2], J.S.S. Scott[2], A. Kovsh[3], V. Ustinov[3], and A. Zhukov[3]

[1] Institut für Angewandte Physik, Universität Regensburg, 93053 Regensburg, Germany
[2] iQuest, University of California at Santa Barbara, CA 93106-5100, USA
[3] Ioffe Institute, St Petersburg 194021, Russia

Received 25 March 2004
Published online 23 July 2004 – © EDP Sciences, Società Italiana di Fisica, Springer-Verlag 2004

Abstract. We report an experimental study indicating ultrafast creation and annihilation of space-charge domains in a semiconductor superlattice under the action of a THz field. Our experiment was performed for an InGaAs/InAlAs superlattice with the conduction electrons undergoing miniband transport. We applied to a superlattice a dc bias that was slightly smaller than a critical bias necessary for the formation of space-charge domains caused by a static negative differential conductivity. Additionally subjecting the superlattice to a strong THz field, resulted in a dc transport governed by the formation of domains if the frequency of the field was smaller than an upper frequency limit (∼3 THz). From this frequency limit for the creation and annihilation of domains we determined the characteristic time of the domain buildup. Our analysis shows that the buildup time of domains in a wide miniband and heavily doped superlattice is limited by the relaxation time due to scattering of the miniband electrons at polar optic phonons. Our results are of importance for both an understanding of ultrafast dynamics of pattern formation in nanostructures and the development of THz electronic devices.

PACS. 72.20.Ht High-field and nonlinear effects – 72.30.+q High-frequency effects; plasma effects – 73.21.Cd Superlattices

1 Introduction

In a semiconductor superlattice the energy an electron can gain moving along the superlattice axis is restricted to minibands [1]. Above a critical field, E_c, conduction electrons, moving in the lowest miniband, give rise to a bulk negative differential conductance (NDC) [1] and to formation of domains [2]. Domains, corresponding to high and low field regions, strongly influence the electron transport through a superlattice. Experimental evidence for domain formation in semiconductor superlattices has been found [3,4]. Propagating dipole domains, created under the influence of a static field producing NDC, have been applied for the generation of microwave radiation via self-sustained current oscillations [5]; radiation with frequencies up to 150 GHz has been observed. Another application represents superlattice frequency multipliers which make use of microwave field induced domain creation and annihilation joint with a nonlinear current response [6,7].

The formation of domains due to the NDC and the emission of radiation by moving domains in semiconductor superlattices has a similarity to the formation of domains due to the Gunn effect in bulk III-V semiconductors [8], however, the physical background for NDC in the superlattice diodes and in Gunn diodes are quite different. The Gunn diodes exhibit NDC caused by intervalley transfer of electrons [9,10], whereas Bragg reflection of miniband electrons is responsible for the NDC in a miniband superlattice [1]. Accordingly, also the dynamics of domain creation and annihilation is quite different.

For bulk semiconductors, two characteristic times govern the rate of growth and collapse of space-charge domains, namely the dielectric relaxation time [11] and the electron relaxation time [12]. The dielectric relaxation time, which is the product of the dielectric constant and the negative specific resistivity [11], is a characteristic constant for the damping of fluctuations in an electric field under normal conditions and their exponential growth in conditions of NDC [11,13]. Its value is typically of the order of 10^{-13} s [13]. The electron relaxation time determines the rate with which the drift velocity of an electron can follow a variation in the electric field [12]. Its value

[a] e-mail: florian.klappenberger@physik.uni-r.de
[b] *Permanent address:* Department of Physical Sciences, P.O. Box 3000, University of Oulu FIN-90014, Finland.

is given by the intervalley relaxation time which is of the order of 1 ps. As Kroemer mentioned, just this longest characteristic time limits the speed of domain formation: For an operation at a frequency larger than the electron scattering rate, domains cannot be created while NDC still can exist [12].

In this paper we are mainly interested in finding the maximum possible speed of formation of domains in semiconductor superlattices. This problem was not treated until now for superlattices exhibiting miniband transport. The driving idea for our measurements is the following. For a superlattice with a miniband width larger than the polar optic phonon energy, the intraminiband relaxation time (∼100 fs) [14] is an order of magnitude shorter than the relaxation time of electrons in Gunn diodes. Therefore, if a characteristic time of domain creation and annihilation in a semiconductor superlattice is controlled by the intraminiband relaxation time, then, an ultimate frequency limit for the operation of active devices based on domains in superlattices can be an order of magnitude faster than for Gunn devices. An upper frequency limit of a few THz follows for superlattice devices in comparison to a few hundred GHz for Gunn devices.

In superlattices, the time characterizing the growth and collapse of space-charge fluctuations is influenced not only by the intraminiband relaxation time, but also by the dielectric relaxation time [2,15]. By analogy with natural bulk semiconductors we suppose that a characteristic time of domain formation in a superlattice, τ_{dom}, is the longest among the intraminiband relaxation time τ and the dielectric relaxation time τ_{diel}, i.e. $\tau_{dom} = \max(\tau, \tau_{diel})$. An estimate shows that $\tau_{diel} \gg \tau$ for semiconductor superlattices having a narrow miniband and small doping. Because the dielectric relaxation time in a superlattice varies inversely proportional to the product of the doping, N, and the miniband width, Δ, i.e. $\tau_{diel} \propto 1/(N\Delta)$, an increase in miniband width and doping results in a decrease of τ_{diel}. In order to measure the shortest of the possible times of domain formation, namely $\tau_{dom} = \tau$, we have chosen an InGaAs/InAlAs superlattice with a very wide miniband and a high doping.

We developed an experimental method which enabled us to study the dynamics of domain formation in a superlattice in a wide frequency range, from 10 GHz to 4 THz. In simple terms, the method consists in a study of the changes of the current-voltage characteristic under the action of a high-frequency field. We found that domain formation caused the current maximum to shift towards smaller voltages and that the shift increased with the ac field amplitude. We observed such kind of shifts for a wide range of frequencies up to several THz. For a large frequency (3.3 THz), the shift disappeared indicating that the miniband electrons did not respond anymore with sufficient speed to the variation of the THz field. Our experimental results contradict predictions following from a *standard miniband transport theory* [16–18], which assumes a homogeneous field distribution in the superlattice. We present a calculation which shows that the homogeneous-field theory predicts the existence of an ac field induced shift in the direction towards larger voltages if $\omega\tau \lesssim 1$ where ω is the angular frequency of the ac field. Further results obtained by simulations in the framework of the drift-diffusion model, as well as an additional experiment on another superlattice, support the main conclusion of the present work: The shortest time of domain formation in a semiconductor superlattice is limited by the intraminiband relaxation time.

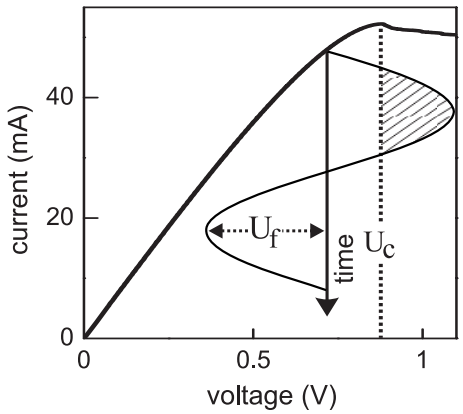

Fig. 1. Measured current-voltage characteristic of an InGaAs/InAlAs superlattice and principle of experiment: Switching the superlattice into a state of negative differential conductivity for a portion (hatched) of the ac field period; U_c, critical voltage and U_f voltage amplitude of the ac field.

The paper is organized as follows. The principle scheme of the experiment, as well as current-voltage (IV) characteristics under the action of a low-frequency field, are presented in the next section. The IV characteristic of superlattices illuminated by THz fields are described in Section 3. Section 4 is devoted to the analysis of experimental results using simulations based on the drift-diffusion model and calculations in the framework of the miniband transport theory. In the final section we summarize and discuss the results of the work.

2 Principle of the experiment

The typical current-voltage characteristic of a heavily doped superlattice exhibits a maximum at a critical voltage, U_c, directly followed by a kink (Fig. 1). For a static voltage, U_s, larger than U_c, electric field domains arise due to NDC. At a bias smaller than the critical U_c, no domains are formed.

We study the change of the IV characteristic of a superlattice under the action of an ac field. Now, the total voltage across the superlattice is $U(t) = U_s + U_f \sin\omega t$ where U_f is the amplitude of the ac voltage. We are mainly interested in the shift of the maximum of the IV curve for $U_f/U_c < 1$. Therefore, we specifically focus on values of U_s that are slightly smaller than U_c (Fig. 1). We will show that domains can be induced by the total voltage $U(t)$ exceeding U_c (Fig. 1, hatched) if the miniband electrons can follow the ac field adiabatically ($\omega\tau \lesssim 1$). Domains collapse during the rest of the period $T = 2\pi/\omega$

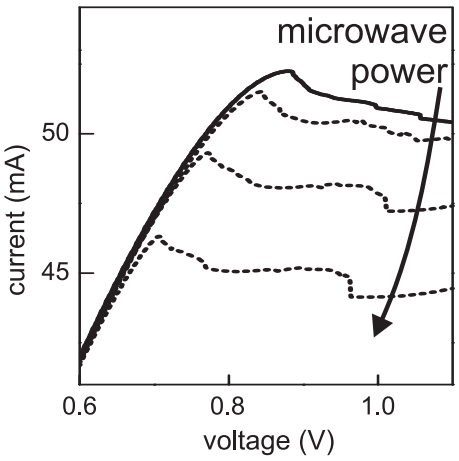

Fig. 2. Current-voltage characteristics of the InGaAl/InAlAs superlattice under the action of a microwave field (frequency 20 GHz, dashed) in comparison with the characteristic of a non irradiated superlattice (solid). The microwave power increases as indicated by the arrow.

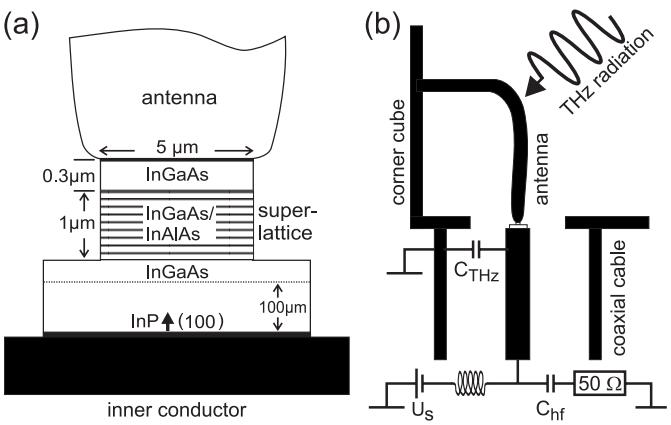

Fig. 3. (a) Sample composition. (b) Cross section of the corner cube with equivalent circuit.

when the total voltage $U(t)$ is smaller than U_c. Whether domains will be really created and annihilated in such conditions or not, depends critically on the relation between the characteristic time of domain buildup, τ_{dom}, and the half-period of the ac field, $T/2$. If $\tau_{dom} < T/2$, domains are formed. However, in the opposite case, $\tau_{dom} > T/2$, a space-charge instability caused by NDC has no time to be fully developed.

We summarize the conditions for periodic formation and annihilation of domains in a superlattice driven by the sum of a dc and an ac voltage: (i) The superlattice has to be driven in the quasistatic regime ($\omega\tau \lesssim 1$), (ii) the NDC condition has to be fulfilled for the total voltage, $U(t) > U_c$, during a part of the period T (while $U_s < U_c$), (iii) τ_{dom} is smaller than the portion of the period during which NDC is possible. We note that a similar experimental method has been used by Pozhela et al. in their investigation of domain buildup in a bulk n-GaAs induced by a microwave field [19,20].

Applying an ac field to a superlattice results in IV characteristics that look quite different in the presence and in the absence of domains. First, we consider the case of a low-frequency ac field. Miniband transport theory, formulated without an account of domain formation, predicts that in the limit $\omega\tau \ll 1$ an application of an ac field results in a shift of the maximum of the IV curve towards larger voltages in comparison with the nonirradiated superlattice [21,22]. This "right shift" is caused by a nonlinearity of the Esaki-Tsu characteristic; the shift increases with increasing ac field amplitude. However, experimental IV curves measured in the presence of a low-frequency field are often looking differently. In Figure 2 typical experimental IV characteristics of a superlattice irradiated by a microwave radiation (frequency 20 GHz, dotted curves) are shown in comparison with the IV characteristic of the nonirradiated superlattice (solid curve). Formation of domains causes the maximum of the IV curve to shift towards smaller voltages; the "left shift" increases with an increase of intensity of the microwave field. In this situation, domains can build up because $\tau_{dom} < T/2$ according to the large period of the low-frequency field. It will be shown in the next section that in a heavily doped superlattice with a very wide miniband domains can be induced by radiation of a frequency as high as few THz.

3 Experiment

In our experiments we studied a very wide miniband superlattice consisting of 120 periods of 4.4 nm thick $In_{0.53}Ga_{0.47}As$ layers separated by 0.9 nm $In_{0.52}Al_{0.48}As$, grown lattice matched on an n^+ InP wafer by use of molecular beam epitaxy (Fig. 3a). The superlattice which was doped with silicon (8×10^{16} cm^{-3}) was embedded between layers of highly doped InGaAs (10^{19} cm^{-3}). Using a modified Kronig-Penney model [23], we calculated the width of the lowest miniband ($\Delta \sim 190$ meV). In an earlier experiment [5], the peak-drift velocity of the miniband electrons ($v_p = 1.5\times10^7$ cm/s) has been determined and it has been shown that propagating domains in the superlattice led to the generation of microwave radiation (150 GHz for this superlattice). From the wafer, a device had been fabricated by photolithography and wet chemical etching. The device consisted of a cylindrical superlattice mesa element (cross-section area 20 μm^2) which had an ohmic contact on top. The bottom was electrically connected to a large contact placed on the InP substrate.

We mounted the superlattice device on the inner conductor of a coaxial cable connected to a metallic corner-cube. An L-shaped antenna was used to electrically connect the superlattice with the corner cube via the top contact (Fig. 3b). We measured the direct current through the device and its dependence on a static voltage, U_s, via the coaxial line and a low-pass filter. We used the Santa Barbara free-electron laser to produce radiation pulses with frequencies from 180 GHz to 4 THz and with a duration of a few μs. We determined the instantaneous THz power from the pulse duration and the pulse energy,

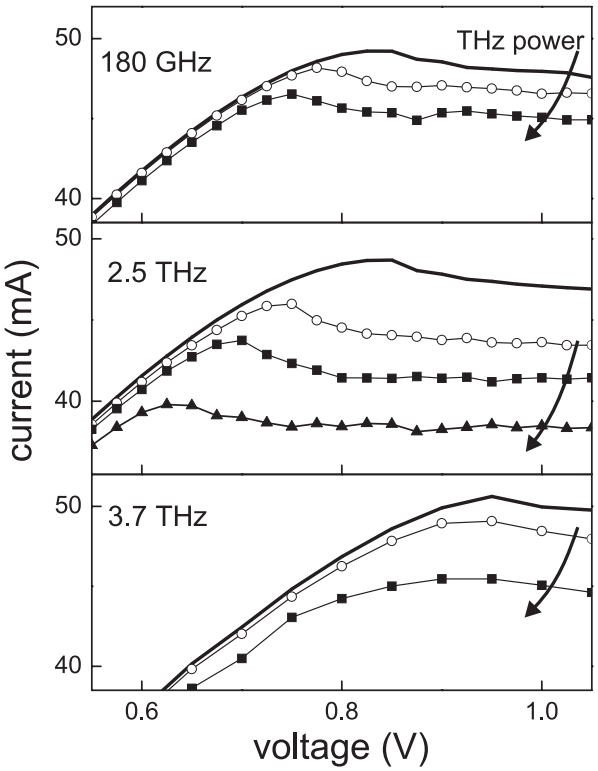

Fig. 4. Current-voltage characteristics of a InGaAs/InAlAs superlattice under the influence of THz radiation (with symbols) in comparison with characteristics of the nonirradiated superlattice (solid). The THz radiation power is increasing as indicated with the arrow.

which we measured with a pyroelectric detector. The THz radiation was coupled quasi-optically to the superlattice device via the antenna and produced a THz current flowing through the sample to the ground via the small capacity, C_{THz}, of the coaxial cable. The THz radiation pulse changed the current through the superlattice giving rise to a current pulse which was transmitted through a large capacity, C_{hf}, and monitored on an oscilloscope as a voltage across an Ohmic resistor (50 Ω). Measurements have been performed for the sample at room temperature.

IV-characteristics of the InGaAs/InAlAs superlattice under the action of THz radiation are shown in Figure 4. THz radiation (frequencies 180 GHz and 2.5 THz) reduced the current at all voltages and caused the current maximum to shift towards smaller voltages in comparison with the nonirradiated superlattice. The shift increased with increasing THz radiation power. Note that similar reduction of the current and a similar "left shift" of the IV curve maximum was observed for frequencies down to 20 GHz (Fig. 2). We attribute the current reduction and the shift of the maximum to the THz field induced formation of domains. The superlattice electrons can respond with sufficient speed to the field and can cause NDC during the positive excursions of the THz field. As the THz field swings back, the NDC disappears. Correspondingly, a charge density domain may have grown during the positive excursions and collapsed during the negative excursions. Accordingly, as the THz power was increased, the positive excursions of the THz field reached the negative differential conductivity region for smaller values of the DC voltage. That is to say, the larger shift indicates that for larger amplitudes of the THz field, an instantaneous voltage in excess of U_c could be reached at a smaller static voltage U_s. Our results demonstrate that the domain formation in the InGaAs/InAlAs superlattice can follow electric-field changes up to a few THz corresponding to creation and annihilation times of the order of 100 fs.

However, for THz radiation with a larger frequency (3.7 THz) the overall current was simply depressed and there was no shift of the IV curve maximum (Fig. 4, lower). The absence of a shift indicates that domains were not induced by the THz radiation at the highest frequency.

We made the same kind of measurement with a GaAs/AlAs superlattice. This superlattice, consisting of 80 periods of 4.9 nm of GaAs and 0.9 nm AlAs, had a miniband width of 70 meV and a doping of 8×10^{16} cm^{-3}. We found that the current maximum shifted towards smaller voltages only under the action of a low frequency radiation (tens of GHz), whereas we observed a shift towards larger voltages for 2 THz radiation. We did not see any visible shifts of the IV curve maximum in the case of radiation at frequencies of 3 and 3.7 THz. These observations indicate that the domain formation time in the GaAs/AlAs superlattice was so that $\tau_{dom} > T/2$ for the case of 2 THz. We attribute the difference in τ_{dom} between the two superlattices mainly to the smaller miniband width of the GaAs/AlAs superlattice which had a miniband width being by a factor of 3 smaller than that of the InGaAs/InAlAs superlattice. The difference of the miniband relaxation times in these two different superlattices played most likely a minor role.

4 Analysis of the experimental results

In this section we will explain the observed shifts of the IV curve maximum under the action of ac fields. In particular, we need to provide a theoretical background for the following results: (i) Domains can induce a shift of the IV curve maximum towards smaller voltages. (ii) The nonlinearity of the IV characteristic alone cannot be the reason for this shift. (iii) Neither domains nor nonlinearity of the IV curve can induce a shift for a very high frequency, $\omega\tau \gg 1$. We treat the problem by using a combination of several different approaches. Namely, we estimate the dielectric relaxation time and compare its value with the intraminiband relaxation time and the period of the ac field. Next, we make use of a drift-diffusion model to simulate changes of the IV curve induced by an ac field and compare the results with results following from the standard miniband transport model. Each of these approaches can provide a sufficient understanding of one of the aspects of the problem, while all approaches have their own range of applicability. For instance, the drift-diffusion model can explain the IV shift due to domains, but it is inapplicable for high frequencies. On the other hand, the standard

miniband transport model works well for any frequency, but it does not allow domain formation. Combining these different approaches, we can well understand the physics underlying our experimental observations.

4.1 Two characteristic times of domain formation in a superlattice

For a single miniband, the dependence of the electron drift velocity, $v(E)$, on an applied static electric field is governed by the Esaki-Tsu relation [1]

$$v(E) = 2v_p \frac{E/E_c}{1+(E/E_c)^2}, \quad (1)$$

where v_p, the peak-drift velocity, is the drift velocity at the critical electric field E_c. The dielectric relaxation time, τ_{diel}, defined by the relation [11,13,24] $\tau_{diel}^{-1} = (4\pi\sigma/\epsilon)\partial v/\partial E$, with account of equation (1) takes the form $\tau_{diel}^{-1} = \omega_{pl}^2 \tau (1-(E/E_c)^2)\left[1+(E/E_c)^2\right]^{-2}$, where σ is the superlattice conductivity, $\omega_{pl} = \left((4\pi e^2 N)/m\epsilon\right)^{1/2}$ is the miniband plasma frequency (N is the number of electrons per cm^3, m the electron mass at the bottom of the miniband, and ϵ the average dielectric constant of the superlattice). We found that in our case the intraminiband relaxation time τ was ∼110 fs. This value is a compromise between the value obtained by fitting the measured IV curves by an Esaki-Tsu characteristic and a value obtained from an analysis of shifts of the IV curve maximum (see Sect. 4.3).

For $E > E_c$ the dielectric relaxation time τ_{diel} becomes negative indicating the growth of space-charge fluctuations under the conditions of NDC. Assuming that the negative differential mobility takes its maximal absolute value 1/8 (at $E/E_c = \sqrt{3}$), we estimated $\tau_{diel} \approx 110$ fs for the InGaAs/InAlAs superlattice. Therefore, τ_{diel} is comparable with τ. Importantly, both τ_{diel} and τ are shorter than the half-period at 2.5 THz ($T/2 = 200$ fs); the values are consistent with the observation that domains are created and annihilated at 2.5 THz (see Fig. 4, middle).

For the GaAs/AlAs superlattice, we found $\tau_{diel} \sim$ 340 fs. Because here $\tau_{diel} > \tau$, the characteristic time of domain formation is determined by τ_{diel}. Thus, for this superlattice τ_{dom} was longer than the half-period already at 2 THz ($T/2 = 250$ fs) resulting in a "right shift" of the IV maximum, which is typical for a superlattice without domain formation (see [21] and Sect. 4.3 below).

4.2 Simulations based on the drift-diffusion model

To demonstrate that a periodic formation of domains in an ac-driven superlattice can result in a shift of the IV maximum towards smaller voltages, we made numerical simulations based on a one-dimensional drift-diffusion model [13,24]. From the continuity and the Poisson equations, the spatio-temporal variation of the electron density, $n(z,t)$, along the superlattice axis was calculated. We introduced an electric-field dependent drift-velocity of electrons in the superlattice following equation (1). The drift-velocity showed a region of negative differential mobility for $E/E_c > 1$. We took into account a diffusion current with the diffusion coefficient given by the Einstein relation. Injection and extraction of electrons into and out of the superlattice was modeled by a cathode and an anode layer which were both characterized by an ohmic mobility lower than the small-field mobility of the superlattice. The doping level in the cathode and anode were chosen equal to the doping in the superlattice. For an applied voltage $U(t) = U_s + U_f \sin\omega t$, we calculated the current through the superlattice with the dielectric current also taken into account.

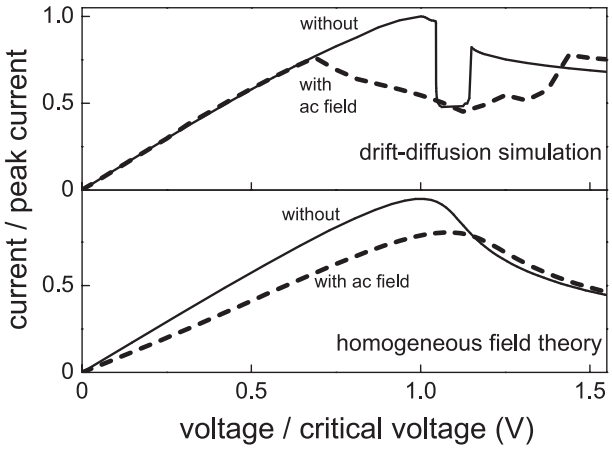

Fig. 5. Current-voltage characteristics calculated in the framework of the drift-diffusion model (upper) and using the standard miniband transport theory (lower). The formation of domains results in a shift of the current maximum to smaller voltages. Assuming a homogeneous field the nonlinear miniband transport produces a shift to larger voltages.

Our simulations show the following picture of domain dynamics. If the instantaneous voltage $U(t)$ exceeds a critical value U_c, a dipole domain starts to build up at the cathode. The dipole domain consists of a depletion layer followed by an accumulation layer and travels through the superlattice towards the anode. The domain grows as long as $U(t) > U_c$ but is annihilated shortly after the voltage drops below U_c. Before a new domain is started, the electron density is constant within the superlattice except for regions close to the cathode and the anode.

Application of an ac field (frequency ∼ 200 GHz) results in formation of domains and in a significant shift of the IV curve maximum towards smaller voltages (Fig. 5, upper). Increasing the ac frequency in the simulation, one finds that the shift disappears, i.e. the maximum occurs at the same voltage for all THz field amplitudes. In the simulation, this change of the behavior is due to a finite dielectric relaxation time τ_{diel}. The drift-diffusion model can qualitatively explain the observed domain-induced "left shift". However, the model is unlikely to be applicable at

THz frequencies. Neither the use of the Einstein relation is reasonably well justified nor the assumption of an instantaneous response, which is determined by the Esaki-Tsu characteristic. For a more sophisticated analysis of the THz frequency range the development of a "generalized drift-diffusion model" would be required [26].

In this respect, it is very instructive to oppose our experimental results to calculations carried out within the miniband transport theory, which is valid for any frequency of the ac field but does not take into account the possibility of domain formation.

4.3 Comparison with results of the miniband transport theory

Our calculations carried out in the framework of the *standard miniband transport theory* [16–18] clearly show the existence of a shift in the direction of larger voltages that is induced by an ac field.

For low frequency ($\omega\tau \ll 1$), the electron drift velocity $v(t)$ can follow adiabatically to changes of the ac electric field $E(t) = E_s + E_f \cos\omega t$. Then, we can substitute the instantaneous electric field $E(t)$ in the Esaki-Tsu equation and after time averaging we obtain for the static electron velocity

$$\overline{v}(E_s, E_f) = \frac{1}{T}\int_0^T v\left(E \to E_s + E_f \cos\omega t\right) dt, \quad (2)$$

where v is defined by equation (1). A typical IV characteristic calculated using equation (2) shows the shift of the current maximum towards larger voltages (Fig. 5, lower). Such a behavior is in contrast with both the results of our drift-diffusion simulations (cf. upper in Fig. 5) and with the experimental results (cf. Fig. 2). Within the quasistatic regime of interaction the value of the shift is a function of the amplitude E_f only and does not depend on the frequency of the ac field. To describe the IV curve of a superlattice under the action of a field with a higher frequency, we use a formula of the standard miniband transport theory

$$\overline{v}(E_s, E_f, \omega) = \sum_{n=-\infty}^{\infty} J_n^2\left(\frac{eaE_f}{\hbar\omega}\right) v\left(E \to E_s + \frac{n\hbar\omega}{ea}\right). \quad (3)$$

We calculated $\overline{v} - E_s$ characteristics for different ac field amplitudes and frequencies. We found the values of E_s^p determining the maximum value of the velocity, $\max(\overline{v})$. We define the relative shift of the IV curve maximum as $S = (E_s^p - E_c)/E_c$. The positive (negative) relative shift indicates that the IV curve maximum shifts towards larger (smaller) voltages. The dependence of the relative shift (in percent) on the frequency and for different values of E_f is shown in Figure 6 (solid). For frequencies up to $\omega\tau \sim 1$, the relative shift is independent of ω; its value is in agreement with the corresponding value calculated using equation (2). For a range of frequencies between $\omega\tau \sim 1$ and $\omega\tau \sim 1.8$, the relative shift first slightly increases and then sharply decreases. Finally, for frequencies larger than $\omega\tau \sim 1.8$, we found a negligibly small negative relative shift. Such a behavior becomes more pronounced at larger ac field amplitudes. The positive shift reveals that electrons in a superlattice respond to a total (quasi)static field that is larger than the bias E_s. The disappearance of this shift for $\omega\tau > 1.8$ shows that miniband electrons then cannot follow the changes of the electric field and classical rectification is impossible.

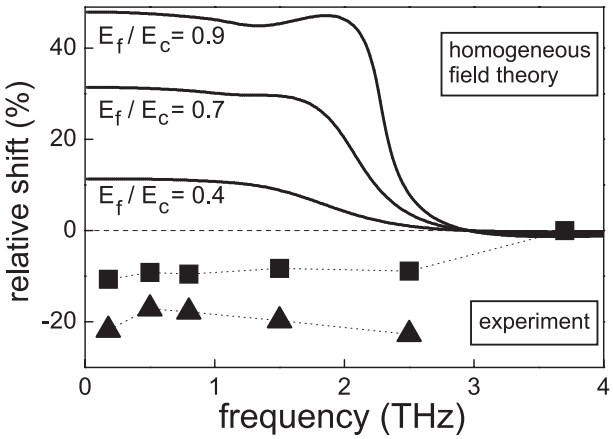

Fig. 6. Dependence of the relative shift of the IV curve maximum on the frequency of the radiation. Observed negative shifts (symbols) are in contrast to positive shifts calculated in the framework of the miniband transport theory (solid lines). A larger THz field amplitude determines a more pronounced shift both in calculations and experiments. Shifts are present in the whole quasistatic frequency range ($\omega\tau \lesssim 1$).

In Figure 6 we also plotted the relative shift of the IV curve maximum, extracted from experimental data (symbols), as a function of the ac field frequency. The experiment shows a negative relative shift in the same range of frequencies that corresponds to the frequency range where a positive shift in the miniband transport model is predicted. A larger THz amplitude (triangles) induces a larger "left shift" compared to the shift induced by a smaller THz amplitude (squares). The nonlinearity of IV curve itself certainly can not be a mechanism providing the observed shift in the whole frequency range. Moreover, the negative shift disappears at the frequency which corresponds to the crossover in the miniband transport theory (accuracy of our measurements of S does not allow to detect an extremely small negative relative shift predicted by theory). It means that domains cannot be created at high frequencies, when the character of the interaction between miniband electrons and THz radiation has changed. We conclude that the ultimate frequency of domain formation is determined by the intraminiband relaxation time τ.

5 Discussion

In conclusion, we reported on changes of the IV characteristic caused by domain formation and annihilation

in a superlattice, which is caused by THz radiation (up to 2.5 THz). We believe that this effect is quite general for heavily doped wide miniband superlattices, where the dielectric relaxation time is less than or of the order of the miniband relaxation time. Our measurements indicate that a characteristic time of domain formation in semiconductor superlattices is limited by the intraminiband relaxation time.

The periodic formation and annihilation of propagating dipole domains in superlattices has been used for the generation of microwave radiation up to 150 GHz [25]. Our present results beg the exploration of "limited space-charge accumulation" (LSA) modes of operation [27,28] in semiconductor superlattices at THz frequencies [29]. This particular domain mode circumvents transit time effects in Gunn diodes, but there, the fundamental limit set by a relatively slow energy relaxation prevents operation above $\sim$100$-$200 GHz. The superlattice system might achieve THz operation that fully uses the fast relaxation by making use of LSA operation. For a better understanding of this regime, it would be necessary to perform more sophisticated simulations that properly include the space-charge and electron dynamics with an account of k-space bunching effects [30,31]. On the other hand, the results of our research are relevant to an understanding the role domains can play in nonlinear processes in semiconductor superlattices, in which a nonlinearity is formed by a dielectric relaxation processes. Corresponding strongly nonlinear phenomena such as bistability [32,33], dynamic chaos [34] and spontaneous symmetry breaking [35,36] have been predicted recently but still were not observed in experiments.

This research was supported by the Deutsche Forschungsgemeinschaft, ONR MFEL program, DARPA/ONR THz Technology program, ARO Science and Technology program, Academy of Finland (grant 1206063), and the Humboldt Foundation.

References

1. L. Esaki, R. Tsu, IBM J. Res. Dev. **14**, 61 (1970)
2. M. Büttiker, H. Thomas, Phys. Rev. Lett. **38**, 78 (1977)
3. H. Le Person, C. Minot, L. Boni, J.F. Palmier, F. Mollot, Appl. Phys. Lett. **60**, 2397 (1992)
4. K. Hofbeck, J. Grenzer, E. Schomburg, A.A. Ignatov, K.F. Renk, D.G. Pavel'ev, Yu. Koschurinov, B.Ya. Melzer, V.M. Ustinov, S.V. Ivanov, S. Schaposchnikov, P.S. Kop'ev, Phys. Lett. A **218**, 394 (1996)
5. E. Schomburg, T. Blomeier, K. Hofbeck, J. Grenzer, S. Brandl, I. Lingott, A.A. Ignatov, K.F. Renk, D.G. Pavel'ev, Yu. Koschurinov, B.Ya. Melzer, V.M. Ustinov, S.V. Ivanov, A. Zhukov, P.S. Kop'ev, Phys. Rev. B **58**, 4035 (1998)
6. R. Scheuerer, M. Haeussler, K.F. Renk, E. Schomburg, Yu.I. Koschurinov, D.G. Pavelev, N. Maleev, V. Ustinov, A. Zhukov, Appl. Phys. Lett. **82**, 2826 (2003)
7. M. Haeussler, R. Scheuerer, K.F. Renk, Yu. Kuschurinov, D.G. Pavel'ev, Electron. Lett. **39**, 628 (2003)
8. J.B. Gunn, Solid State Commun. **1**, 88 (1963)
9. B.K. Ridley, T.B. Watkins, Proc. Phys. Soc. Lond. **78**, 293 (1961)
10. H. Kroemer, Proc. IEEE **52**, 1736 (1964)
11. A.L. Zakharov, Zh. Eksp. Teor Fiz. **38**, 665 (1960) [Sov. Phys. JETP **11**, 478 (1960)]
12. H. Kroemer, Proc. IEEE **53**, 1246 (1965)
13. B.R. Pamplin, Contemp. Phys. **11**, 1 (1970)
14. S. Winnerl, E. Schomburg, J. Grenzer, H.-J. Regl, A.A. Ignatov, A.D. Semenov, K.F. Renk, D.G. Pavel'ev, Yu. Koschurinov, B.Y. Melzer, V.M. Ustinov, S.V. Ivanov, S. Schaposchnikov, P.S. Kop'ev, Phys. Rev. B **56**, 10303 (1997)
15. A.A. Ignatov, V.I. Shashkin, Zh. Eksp. Teor. Fiz. **93**, 935 (1987) [Sov. Phys. JETP **66**, 526 (1987)]
16. A.A. Ignatov, Yu.A. Romanov, Phys. Status Solidi (b) **73**, 327 (1976)
17. V.V. Pavlovich, É.M. Épshteĭn, Fiz. Tekh. Polupr. **10**, 2001 (1976) [Sov. Phys. Semicond. **10**, 1196 (1976)]
18. A.A. Ignatov, E. Schomburg, J. Grenzer, K.F. Renk, E.P. Dodin, Z. Phys. B **98**, 187 (1995)
19. T.Ya. Banis, I.V. Parshelyunas, Yu.K. Pozhela, Fiz. Tekh. Polupr. **5**, 1990 (1971) [Sov. Phys. Semicond. **5**, 1727 (1972)]
20. T.Ya. Banis, I.V. Parshelyunas, Yu.K. Pozhela, Lietuvos Fiz. Rink. (Lithuanian Phys. J.) **11**, 1013 (1971)
21. S.Y. Mensah, J. Phys.: Condens. Matter **4**, L325 (1992)
22. A.A. Ignatov, Yu.A. Romanov, Izv. VUZ Radiofiz. **21**, 132 (1978) [Radiophysics and Quantum Electronics (Consultants Bureau, New York) **21**, 91 (1978)]
23. G. Bastard, *Wave Mechanics Applied to Semiconductor Heterostructures* (Les Éditions de Physique, Les Ulis, 1988)
24. A.F. Volkov, S.M. Kogan, Usp. Fiz. Nauk **96**, 633 (1968) [Sov. Phys.-Usp. **11**, 881 (1969)]
25. E. Schomburg, R. Scheuerer, S. Brandl, K.F. Renk, D.G. Pavelev, Y. Koschurinov, V.M. Ustinov, A. Zhukov, A. Kovsh, P.S. Kopev, Electron. Lett. **35**, 491 (1999)
26. L.L. Bonilla, R. Escobero, A. Perales, Phys. Rev. B **68**, 241304 (2003)
27. J. Copeland, Proc. IEEE **54**, 1479 (1966)
28. J. Copeland, J. Appl. Phys. **38**, 3096 (1967)
29. H. Kroemer, `cond-mat/0009311`
30. H. Kroemer, `cond-mat/0007482`
31. E. Schomburg, N.V. Demarina, K.F. Renk, Phys. Rev. B **67**, 155302 (2003)
32. A.W. Ghosh, A.V. Kuznetsov, J.W. Wilkins, Phys. Rev. Lett. **79**, 3494 (1997)
33. E.P. Dodin, A.A. Zharov, A.A. Ignatov, Zh. Eksp. Teor. Fiz. **114**, 2246 (1998) [JETP **87**, 1226 (1998)]
34. K.N. Alekseev, G.P. Berman, D.K. Campbell, E.H. Cannon, M.C. Cargo, Phys. Rev. B **54**, 10625 (1996)
35. K.N. Alekseev, E.H. Cannon, J.C. McKinney, F.V. Kusmartsev, D.K. Campbell, Phys. Rev. Lett. **80**, 2669 (1998)
36. K.N. Alekseev, E.H. Cannon, F.V. Kusmartsev, D.K. Campbell, Europhys. Lett. **56**, 842 (2001)